Executive Summary of the Thesis

Benchmark of the TDT MOC-3D solver of APOLLO3® against Serpent during depletion

Laurea Magistrale in Nuclear Engineering - Ingegneria Nucleare
Scuola di Ingegneria Industriale e dell'Informazione

Author: Matteo Montanari

Advisor: Prof. Stefano Lorenzi

EDF Supervisor: Dr. Marco Tiberga

CEA Supervisors: Dr. Simone Santandrea
Dr. Andrea Gammicchia

Academic year: 2024-2025

1. Introduction

Achieving one-step core calculations requires continuous improvements in deterministic neutron transport solvers. Significant progress has been made with the TDT (Two-Three Dimensional Transport) solver of APOLLO3®, the next-generation multi-purpose code developed at CEA. Based on the Method of Characteristics (MOC), TDT was recently extended to full 3D for extruded geometries.

To reduce computational cost and memory consumption, an axial polynomial expansion for the neutron flux was introduced. However, as burnup progresses, macroscopic cross sections develop strong axial gradients, especially at reflector interfaces, that low-order methods cannot accurately capture. To handle depleted systems while preserving efficiency, this higher-order axial treatment has been extended to macroscopic cross sections [1].

Building on previous benchmarks against TRIPOLI-4® for a standard PWR UOX assembly up to 60 GWd/tHM [4], this work assesses the TDT MOC-3D solver against the Serpent Monte Carlo code [3], which offers higher precision for depletion performance with respect to TRIPOLI-4®. The analysis includes also UOX-Gd assemblies from the PRATIC core, part of the EASI-SMR initiative [5].

1.1. Description of the assemblies

The primary aim of this work is to accurately benchmark the TDT MOC-3D solver of APOLLO3® along depletion for a PWR assembly with UOX fuel enriched at 3.7 % in mass. Radially, it features a 17×17 lattice in an all-rods-out configuration with a central instrumentation channel. Due to symmetry, only one-eighth of the lattice was simulated using reflective boundaries (see Figure 1), reflective ones at the mid-plane (2.25 m) and vacuum conditions beyond the reflector. Fuel rods were divided into four concentric rings to accurately model burnup evolution. Axially, the 3.92 m active height assembly includes six Zircaloy grids and a 29 cm axial reflector composed of homogenized water-steel layers, as shown in Figure 1c. All materials are set at 624 K to match the JEFF-3.1.1 nuclear data library.

For the UOX-Gd assemblies, the study aims to confirm the robustness of APOLLO3® regarding gadolinium concentration. Two configurations were chosen: one with 36 UOX-Gd rods (enriched at 3.5 wt%) and another with 8 (2.5 wt%) as illustrated in Figure 2. In these cases, grids are not modeled and both temperature and nuclear data library are the same of the UOX case. Each fuel axial layer is 10.0281 cm thick and the reflectors are 5 cm, resulting in a total height of 120.2807 cm (Figure 2c).

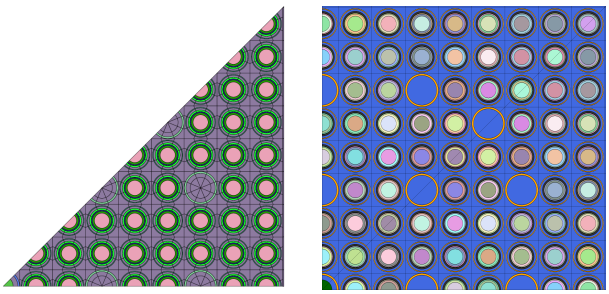

(a) APOLLO3®. (b) Serpent.

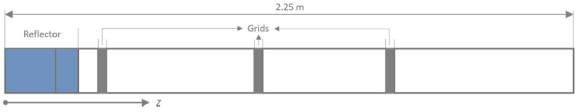

(c) Vertical layout (from [1]).

Figure 1: Radial layout and vertical cut of the 3D PWR UOX assembly.

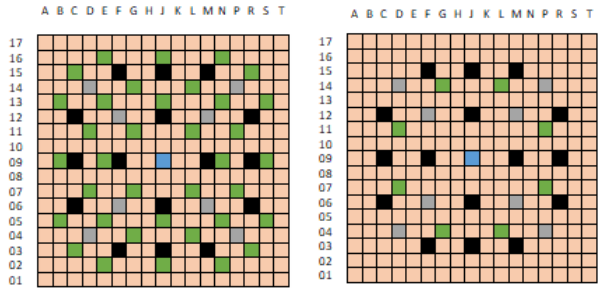

(a) 36 UOX-Gd rods. (b) 8 UOX-Gd rods.

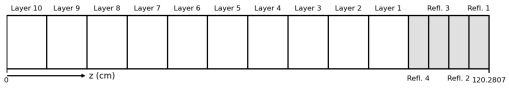

(c) Vertical layout (36 UOX-Gd).

Figure 2: X-Y and vertical cuts of the PRATIC UOX-Gd assemblies.

2. Convergence analysis

A detailed convergence analysis was performed to identify optimal computational parameters for APOLLO3® and Serpent, balancing precision and efficiency in depletion simulations. For the former, the strategy involved starting with existing radial and axial meshes [4], studying TDT MOC-3D flux solver parameter impacts at zero burnup, refining the radial mesh, and comparing depletion results against Monte Carlo references in terms of k_{eff} , fission and capture rates. While for the latter, the analysis involved a preliminary axial and burnup mesh convergence test.

2.1. APOLLO3®, UOX assembly

A development version of APOLLO3® based on v3.1 was used with nuclear data condensed in 281 groups from the CEAV514 library. Calculations employed a maximum anisotropy order $K = 3$, polynomial order $N_p = 2$, and a predictor-corrector method with 4 substeps for burnup, with self-shielding calculated at each step using the Fine Structure model and the Livolant-Jeanpierre method for the resonant mixture treatment. Flux calculations were performed setting a precision of 10^{-5} for the eigenvalue, thermal, and inner iterations, and 10^{-4} for the fission integral.

MOC-3D tracking parameters tested included azimuthal angles N_φ, polar angles N_θ, transversal step size in the x-y plane Δ_{xy}, and axial step size Δ_z. Results reported in Table 1 showed that k_{eff} remained stable for N_θ and Δ_z, while N_φ required careful attention due to interdependencies with Δ_{xy}. For each parameter, the run with the most accurate value is selected as the reference case. All other results are then compared with this reference by computing the relative difference $(\frac{k_{eff}}{k_{effref.}} - 1)$ in pcm. Values in bold correspond to the initial options adopted. Cross-parameter studies revealed that $N_\varphi = 30$ with $\Delta_{xy} = 0.03\,\text{cm}$ ensured convergence and was adopted as the default setup, as shown in Table 2.

Table 1: TDT MOC-3D parameters convergence analysis.

Param.	Set 1	Set 2	Set 3	Set 4	Set 5	Set 6
N_φ	18	20	**24**	30	36	-
k_{eff}	1.29573	1.29570	1.29603	1.29605	1.29626	-
Rel. diff.	*(-41)*	*(-43)*	*(-18)*	*(-16)*	*ref*	-
N_θ	**4**	5	-	-	-	-
k_{eff}	1.29603	1.29607	-	-	-	-
Rel. diff.	*(-3)*	*ref*	-	-	-	-
Δ_{xy}	0.01	0.02	0.03	**0.05**	0.06	0.07
k_{eff}	1.29610	1.29611	1.29606	1.29603	1.29607	1.29587
Rel. diff.	*ref*	*(1)*	*(-3)*	*(-5)*	*(-2)*	*(-18)*
Δ_z	0.1	0.2	**0.3**	0.4	0.5	0.7
k_{eff}	1.29602	1.29602	1.29603	1.29602	1.29603	1.29601
Rel. diff.	*ref*	*(0)*	*(1)*	*(0)*	*(1)*	*(-1)*

The radial mesh was improved using a *windmill* configuration with 8 sectors in guide tubes to better model flux thermalization at cell corners (Figure 1a).

2.2. Serpent, UOX assembly

Serpent-2.2.1 [3] was executed in maximum performance mode with the CRAM burnup method, using unresolved probability table sampling, and adopting the LELI predictor-

Table 2: TDT coupled parameters analysis.

Param.	Set 1	Set 2	Set 3
N_φ–Δ_{xy}	20-0.01	20-0.02	**24-0.05**
k_{eff}	1.29589	1.29588	1.29603
Rel.diff.	*(-17)*	*(-18)*	*(-6)*
	30-0.02	30-0.03	30-0.04
	1.29611	1.29612	1.29610
	ref	*(1)*	*(-1)*
N_θ–Δ_z	**4-0.3**	5-0.1	5-0.2
k_{eff}	1.29603	1.29606	1.29608
Rel.diff.	*(-4)*	*(-2)*	*ref*

Table 3: Analysis with $\Delta_{xy} = 0.03$.

Param.	Set 1	Set 2	Set 3
N_θ	**4**	5	-
k_{eff}	1.29606	1.29612	-
Rel.diff.	*(-5)*	*ref*	-
Δ_z	0.2	**0.3**	0.4
k_{eff}	1.29607	1.29606	1.29607
Rel.diff.	*ref*	*(-3)*	*(0)*
N_θ–Δ_z	**4-0.3**	5-0.2	-
k_{eff}	1.29606	1.29611	-
Rel.diff.	*(-6)*	*ref*	-

corrector approach with 3 predictor and 5 corrector substeps, as suggested in [2]. The nuclear library was adjusted to match APOLLO3®'s CEAV514 library: the 52 additional nuclides sourced from other libraries were removed from Serpent's .xsdata file, except for ^{253}Cf from ENDF/B-VII which is also present in the CEAV514 library. The Doppler-broadening was used to pre-process nuclides data at 600 K.
For the axial mesh convergence, simulations were performed with varying numbers of layers. A compromise between k_{eff} accuracy and computational feasibility was required due to HPC cluster time constraints, namely decreasing the neutron population as the number of layers increased was necessary, as reported in Table 4. Inactive cycles always remained 300.

Table 4: Parameters of Serpent simulations for the axial mesh convergence analysis.

BU zones	Fuel layers	set pop ($\times 10^3$)	$\sigma(k_{eff})$ (pcm)
1099 (material mesh)	7	100 / 30	1.8
4082	26	200 / 9.5	2.3
7065	45	200 / 8	2.5
1208 (step mesh)	77	200 / 6	2.9

The 7065-zone, 45-fuel layer configuration (Figure 3) was identified as converged, defined as relative k_{eff} differences fluctuating around zero within 3σ intervals, as illustrated in Figure 4. The layering strategy used finer meshes near interfaces to capture flux gradients.

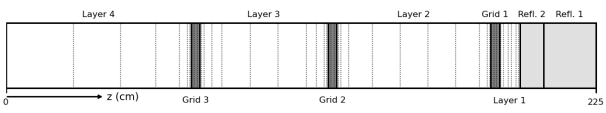

Figure 3: Serpent: Fuel rod axial subdivision in 45 axial layers plus 2 reflector ones.

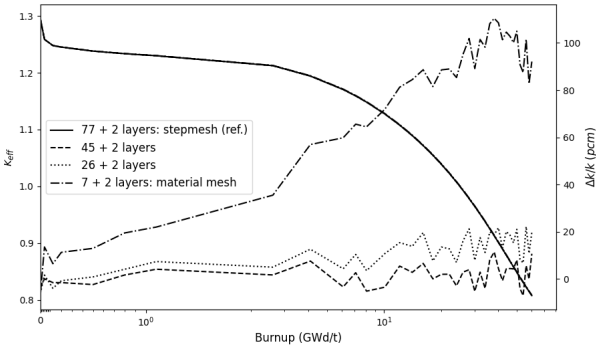

Figure 4: Convergence of k_{eff} varying axial mesh (solid line: k_{eff} values; dashed lines: relative errors.)

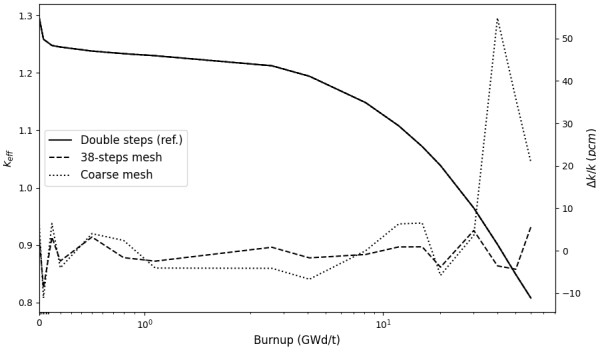

Figure 5: Verification of the converged burnup mesh (solid line: k_{eff} values; dashed lines: relative errors.)

Regarding the burnup mesh, the 38-step configuration was derived from the industrial step size limit of 2 GWd/tHM. The selected steps (in GWd/tHM) are: 0.0, 0.04, 0.12, 0.2, 0.5, 0.8, 1, 2, 4, 5.5, 7, 8.5, 10, and thereafter in constant increments of 2 GWd/tHM up to 60 GWd/tHM. This configuration was confirmed to remain statistically consistent with finer meshes, whereas coarser meshes failed to converge (Figure 5).

2.3. UOX-Gd assembly

The same convergence procedure (not exhaustively reported for the sake of conciseness) was applied to the 36 UOX-Gd assembly, whose radial mesh is shown in Figure 6. The radial mesh featured 11 subdivisions in gadolinium-containing rods to correctly model the skin effect.
Figure 7 reports the axial subdivision that consisted of 10 fissile layers and 4 reflector layers for the material mesh, subdivided into 30 axial layers for Serpent.
A finer burnup mesh (comprising 61 steps) was required for the UOX-Gd case due to

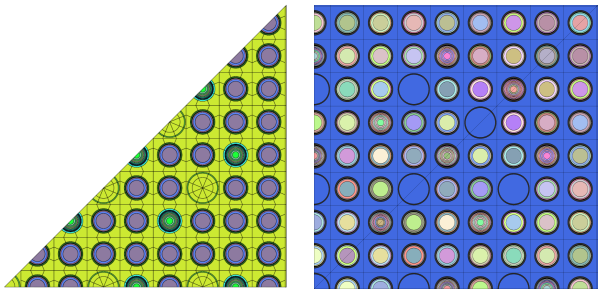

(a) APOLLO3®, x-y layout (36 UOX-Gd). (b) Serpent, x-y layout (36 UOX-Gd).

Figure 6: Radial layout (a,b) of the 3D PWR 36 UOX-Gd assembly case.

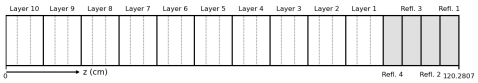

Figure 7: Serpent: Fuel rod axial subdivision in 30 axial layers plus 4 reflector ones.

gadolinium's high neutron capture cross section, which causes steep flux gradients. The selected steps (in GWd/tHM) are: 0.0, 0.018 75, 0.1125, 0.2375, 0.5, 0.75, 1.25, 1.75, 2.5, 3.0, 3.75, 4.25, 5.0, 5.25, 5.5, 5.875, 6.25, 6.5, 6.75, 7.125, 7.5, 7.75, 8.0, 8.375, 8.75, 9.0, 9.25, 9.625, and 10.0. From this point, the mesh is relaxed to steps of 0.5 up to 12.0 GWd/tHM, steps of 1.0 up to 20.0 GWd/tHM, and finally steps of 2.0 up to 60.0 GWd/tHM.

The burnup steps are finer than the UOX case because gadolinium's high neutron capture cross section causes steep flux gradients, requiring more refined mesh resolution. The same radial, burnup, and axial meshes were adopted for the 8 UOX-Gd case to ensure consistency and avoid performing another convergence analysis.

3. Serpent - APOLLO3® depletion benchmark

Comparisons between APOLLO3® and Serpent on the PWR UOX assembly test case depleting up to 60 GWd/tHM required several modifications for improved agreement. In APOLLO3®, the reflector layers were subdivided into two equally spaced layers to improve flux convergence and reduce capture rate error, and two burnup steps at 0.02 and 0.08 GWd/tHM were added to better model xenon buildup and its thermal neutron absorption. Additionally, both codes changed the energy deposition model to normalize at each burnup step only with fission energy (193.7201 MeV for ^{235}U in APOLLO3® library), since default normalization options differed.

Results obtained in terms of k_{eff}, shown in Figure 8, were derived by averaging Serpent results over 20 independent runs with different seeds (each with 4000 batches and 200 000 neutrons each and 300 inactive cycles, yielding $\sigma(k_{eff}) = 3.5$ pcm) to control the statistical uncertainty originating from the Monte Carlo neutronics. The comparison shows generally low relative error, exceeding only 100 pcm between 20 and 40 GWd/tHM with a peak of about 140 pcm at 30 GWd/tHM.

Figure 9 illustrates radially integrated, one-group fission and capture reaction rates normalized to the total fission rate. Vertical light gray lines correspond to material layers (cf. Figure 1c), while gray bars centered at zero relative error represent the 3σ Monte Carlo statistical absolute uncertainty. Largest relative errors occur in the first two active layers near reflectors, while remaining layers exhibit much smaller discrepancies. Pin-wise reaction rates were also analyzed and revealed maximum discrepancies of 2.9% for fission and 4.8% for capture in the first grid layer. The pin-wise distribution of relative error on axially integrated one-group reaction rates at 60 GWd/tHM (Figure 10) shows maximum discrepancy lower than 0.1% for fission rate and around 0.15% for capture, with mean discrepancy ten times lower for the latter.

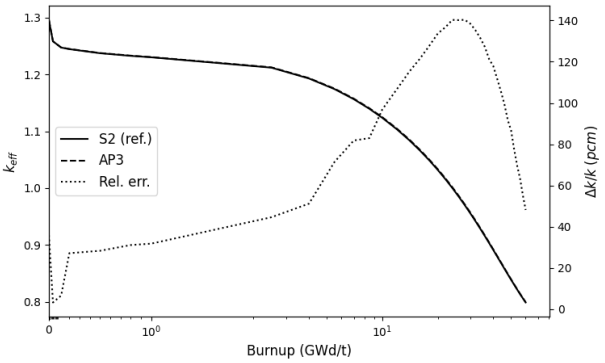

Figure 8: APOLLO3® vs. Serpent comparison: evolution of k_{eff} and relative error during depletion.

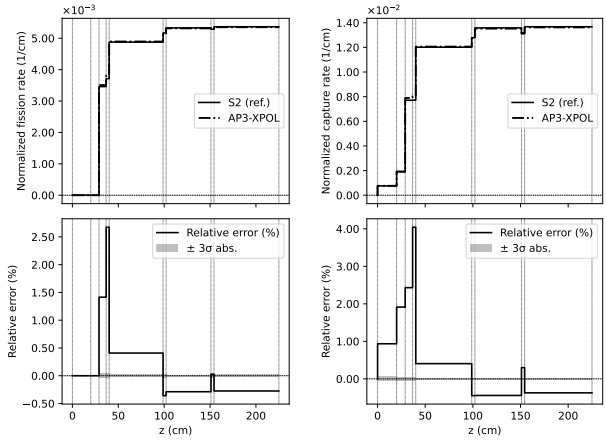

(a) Fission rates (b) Capture rates

Figure 9: APOLLO3® vs. Serpent comparison: radially integrated reaction rates at 60 GWd/tHM (end of life).

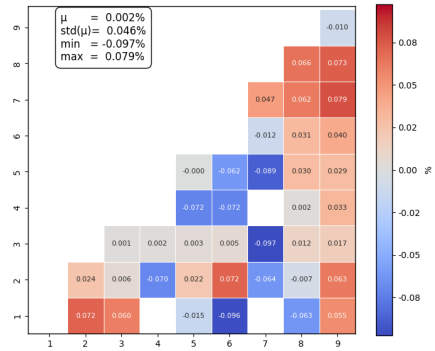

(a) Fission rate error.

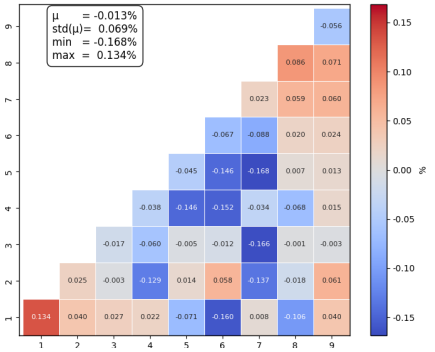

(b) Capture rate error.

Figure 10: Distribution of relative error on axially integrated reaction rates at 60 GWd/tHM ($3\sigma \approx 0.2\%$). UOX assembly test case.

3.1. UOX-Gd assembly

The comparison between Serpent and APOLLO3® at zero burnup for the 36 UOX-Gd fuel assembly showed significant discrepancy in k_{eff} (−467.189 pcm) where Serpent (reference) gives 0.919 26 (σ = 4.1 pcm) and APOLLO3® 0.914 96. This large zero-burnup difference led to even larger relative differences in depletion, as reported in Figure 11.

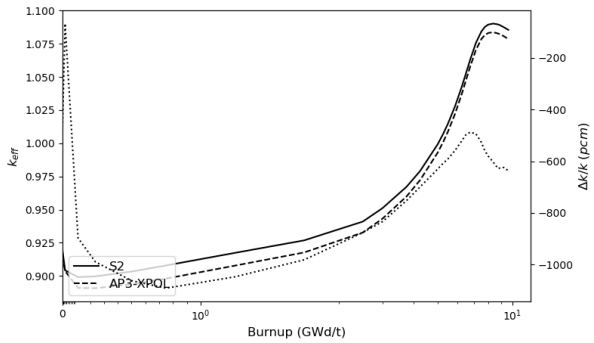

Figure 11: Depletion analysis of the 36 UOX-Gd assembly: benchmark comparison up to 10 000 MWd/tHM between Serpent (reference) and APOLLO3®.

The simulation terminated at 9625 MWd/tHM instead of reaching 60 000 MWd/tHM due to APOLLO3® computational slowness, consuming 14 days at the HPC cluster time limit. These issues prompted a strategic change: analysis was stopped before 60 000 MWd/tHM for both codes, with Serpent rerun using 200 000 neutrons per batch and 4000 batches, yielding k_{eff} uncertainty of 3.5 pcm. The 8-rod UOX-Gd assembly was analyzed directly with the new energy deposition model to reduce discrepancies.

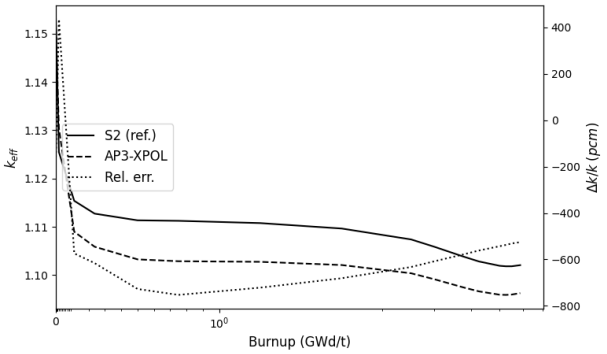

Figure 12: APOLLO3® vs Serpent (up to 5875 MWd/tHM) for the 8 UOX-Gd case with the new energy deposition model.

The benchmark for the 8 UOX-Gd assembly (averaged over 15 independent Serpent simulations) shows in Figure 12 highest relative difference of −753 pcm at 750 MWd/tHM, considerably improved compared to the 36 UOX-Gd case (−1100 pcm). Strong fluctuations occurred in the first three burnup steps, with the second relative error considerably higher than the first and third, though after these initial steps the

trend stabilized.

4. Conclusions

For the UOX assembly, results revealed good agreement between the two codes: k_{eff} discrepancy is very small throughout depletion, with a peak of about 140 pcm at 30 000 MWd/tHM. Relative errors on one-group fission and capture rates are excellent, remaining within 0.5 % in internal axial layers for radially integrated rates and below 0.15 % for axially integrated ones. Remaining k_{eff} deviations likely stem from differences in depletion chains between codes.
For the gadolinium cases, poor results revealed the necessity of the Linear Surface MOC method on the radial plane due to gadolinium's high neutron capture cross section causing steep flux gradients not well represented by the solver. APOLLO3® requires significant computational time, preventing calculations from reaching completion. The 36 UOX-Gd case showed k_{eff} relative differences exceeding 1000 pcm at 750 MWd/tHM, while the 8 UOX-Gd assembly reduced discrepancies to values not greater than −753 pcm. Precision decreases with increasing gadolinium content, making LS method implementation essential.
Regarding perspectives, the UOX case could benefit from further subdivision of the first two fissile layers near reflectors to reduce discrepancies in integrated fission and capture rates, and investigation of depletion chain differences between codes could assess their impact. For gadolinium, focus should be on implementing the LS method within APOLLO3® to improve agreement and reduce computational cost.

5. Acknowledgements

The author would like to thank the APOLLO3® development team for their efforts in developing the code. APOLLO3® is a registered trademark of CEA and is developed with the support of EDF and Framatome. This work received financial support from the European Union's Horizon Europe Research and Innovation program through the EASI-SMR project (Grant Agreement No. 101 164 810).

References

[1] Andrea Gammicchia. *Development and acceleration of a 3D characteristics method including an axial polynomial expansion of cross sections*. Theses, Université Paris-Saclay, September 2021.

[2] Aarno Isotalo. *Computational methods for burnup calculations with Monte Carlo neutronics*. PhD thesis, Aalto University, 2013.

[3] Jaakko Leppänen et al. Status of serpent monte carlo code in 2024. *EPJ - Nuclear Sciences & Technologies*, 11, 2025.

[4] Simone Santandrea et al. Camivver – assessment of new advanced 2d and 3d models in neutronic multi-parameter library generation. Deliverable D4.6, CEA, EDF, Framatome, 2020 - 2023.

[5] Romain Vuiart et al. Pratic: A soluble-boron-free, pressurized water cooled, smr core benchmark. *EPJ - Nuclear Sciences & Technologies*, 10, 2024.